Constraining Cosmological Parameters by the Cosmic Inversion Method

Noriyuki KOGO[1,2,*], Misao SASAKI[2,**] and Jun'ichi YOKOYAMA[3,***]

[1]*Department of Earth and Space Science, Graduate School of Science,*
Osaka University, Toyonaka 560-0043, Japan
[2]*Yukawa Institute for Theoretical Physics, Kyoto University,*
Kyoto 606-8502, Japan
[3]*Research Center for the Early Universe, School of Science,*
The Univeresity of Tokyo, Tokyo 113-0033, Japan

We investigate the question of how tightly we can constrain the cosmological parameters by using the "cosmic inversion" method in which we directly reconstruct the power spectrum of primordial curvature perturbations, $P(k)$, from the temperature and polarization spectra of the cosmic microwave background (CMB). In a previous paper, we suggested that it may be possible to constrain the cosmological parameters using the fact that the reconstructed $P(k)$ does not depend on how many polarization data we incorporate in our inversion procedure if and only if the correct values of the cosmological parameters are used. The advantage of this approach is that we need no assumption regarding the functional form of $P(k)$. In this paper, we estimate typical errors in the determination of the cosmological parameters when our method is applied to the PLANCK observation. We investigate constraints on h, Ω_b, Ω_m, and Ω_Λ through Monte Carlo simulations.

§1. Introduction

The cosmic microwave background (CMB) is one of the most powerful tools to determine the values of the cosmological parameters and examine the properties of the primordial fluctuations. A number of observations have been carried out since the Cosmic Background Explorer (COBE) observation.[1] In particular, a recent precise observation made using the Wilkinson Microwave Anisotropy Probe (WMAP) has confirmed that our universe is consistent with a spatially flat ΛCDM universe with Gaussian, adiabatic, and nearly scale-invariant primordial fluctuations, as predicted by a simple slow-roll inflation model.[2]–[5]

Nevertheless, it has been suggested that the primordial power spectrum of the curvature perturbation, $P(k)$, may have some nontrivial features, such as a lack of power on large scales, running of the spectral index, and oscillatory behavior of the spectrum on intermediate scales. Therefore, a conventional parameter-fitting method, in which one often assumes a simple functional form of $P(k)$, such as a power-law spectrum, is unsatisfactory. Instead we need to examine $P(k)$ directly from observations without any theoretical prejudice. For this purpose, there have been several attempts to reconstruct the primordial spectrum using the WMAP data

*) E-mail: kogo@yukawa.kyoto-u.ac.jp
**) E-mail: misao@yukawa.kyoto-u.ac.jp
***) E-mail: yokoyama@resceu.s.u-tokyo.ac.jp

using model-independent methods.[6]–[12]

Cosmic inversion is a method to reconstruct the primordial spectrum directly from CMB anisotropies. It was originally proposed by Matsumiya et al. (2002, 2003).[13],[14] We applied this method to the WMAP first-year data and showed that there are possible nontrivial features of $P(k)$.[15] Our method can reproduce fine features of $P(k)$ with a resolution of $\Delta k \simeq 3.7 \times 10^{-4}\,\mathrm{Mpc}^{-1}$, which roughly corresponds to $\Delta \ell \simeq 5$ in the angular power spectrum, C_ℓ. In a previous work, we improved our method in such a manner that we can use the auto-correlations of both CMB temperature fluctuations (TT) and E-mode polarization (EE).[16] With polarization, we have shown that large numerical errors in the reconstructed $P(k)$ due to the singularities in the inversion formula, which correspond to zero points of the transfer functions, can be suppressed. As a result, we were able to reconstruct $P(k)$ with an error of a few percent in the ideal situation that observational errors do not exist. We have also found that it may be possible to constrain the cosmological parameters by varying the contribution of the polarization in the inversion formula and requiring that the resultant $P(k)$ is independent of the contribution of the polarization. In a conventional parameter-fitting method, it appears that one can determine the cosmological parameters up to a few percent from recent WMAP data. However, this is because the functional space of $P(k)$ is restricted by the assumption of a simple functional form. As a result, these values of the cosmological parameters depend on this assumption. On the other hand, if we regard $P(k)$ as a free function to be reconstructed, there remains the degeneracy that varying the shape of $P(k)$ can compensate for the variation of the cosmological parameters.[17],[18] Therefore, it is important to investigate how well we can determine the cosmological parameters without any assumption on the functional form of $P(k)$.

In this paper, we examine the proposition of determining the cosmological parameters by using the cosmic inversion method. We first confirm that it is possible to determine the cosmological parameters quite accurately when there is no observational error. Then we add artificial observational errors assuming the PLANCK observation[*] and estimate probability distributions of the cosmological parameters by performing Monte Carlo simulations for each set of the cosmological parameters.

This paper is organized as follows. In §2, we review our cosmic inversion method that employs both the CMB temperature and polarization spectra. We also extend it to a nonflat universe and examine the effect of observational errors on the reconstructed $P(k)$. In §3, we describe a new method to constrain the cosmological parameters by using our cosmic inversion method and report the results of simulations to estimate the errors on the cosmological parameters. Finally, we present our conclusion in §4.

---

[*] http://www.rssd.esa.int/index.php?project=PLANCK

§2. Inversion method

2.1. *Formula*

First we present the formula to reconstruct $P(k)$ using both the CMB temperature and polarization spectra.[13), 14), 16)] For completeness, its derivation is described in Appendix A. We consider only scalar-type perturbations in which B-mode polarization is absent, and assume Gaussian and adiabatic primordial fluctuations throughout this paper.

The angular power spectrum of the CMB anisotropy, $C_\ell^{X\bar{X}}$ [where X and $\bar{X}$ are either the temperature fluctuations (T) or the E-mode polarization (E)], and the primordial power spectrum of the curvature perturbation, $P(k)$, are related as

$$C_\ell^{X\bar{X}} = \frac{2}{\pi} \int_0^\infty \frac{dk}{k} \, k^3 P(k) \, K_\ell^{X\bar{X}}(\eta_0, k), \tag{2·1}$$

where $K_\ell^{X\bar{X}}(\eta_0, k)$ is the kernel specified by the Boltzmann equation. As we see, this is an integral equation for $P(k)$. To solve it, we first tentatively adopt the following two approximations. One is the thin last scattering surface (LSS) approximation, in which we perform the time integration of the transfer functions within the thickness of the LSS. The other is the small angle approximation, in which we introduce the new variable $r = 2d \sin(\theta/2)$, which represents the conformal distance between two points on the LSS. With these assumptions, we obtain a first-order differential equation for $P(k)$ from the TT spectrum and algebraic equations for $P(k)$ from the EE and TE spectra, respectively. However, they all have singularities corresponding to the zero points of the transfer functions that relate the primordial curvature perturbation to the temperature and polarization multiple moments. The presence of these singularities leads to large numerical errors near them in the reconstructed $P(k)$, particularly when observational errors are taken into account.

To avoid this difficulty, we construct a linear combination of the TT and EE formulas, introducing a free parameter α, as

$$-k^2 f^2(k) P'(k) + \left[-2k^2 f(k) f'(k) + k g^2(k) + \alpha k h^2(k) \right] P(k)$$
$$= S^{TT}(k) + \alpha S^{EE}(k), \tag{2·2}$$

where $f(k)$, $g(k)$, and $h(k)$ are time-integrated transfer functions within the thickness of the LSS, and the source functions are defined by

$$S^{TT}(k) \equiv 4\pi \int_0^\infty dr \, \frac{1}{r} \frac{\partial}{\partial r} \left\{ r^3 \sum_{\ell=\ell_{\min}}^{\ell_{\max}} \frac{2\ell+1}{4\pi} \frac{C_\ell^{TT,\text{obs}}}{b_\ell^{TT,(0)}} P_\ell \left(1 - \frac{r^2}{2d^2} \right) \right\} \sin kr, \tag{2·3}$$

$$S^{EE}(k) \equiv 4\pi \int_0^\infty dr \, r \sum_{\ell=\ell_{\min}}^{\ell_{\max}} \frac{2\ell+1}{4\pi} \frac{(\ell-2)!}{(\ell+2)!} \frac{C_\ell^{EE,\text{obs}}}{b_\ell^{EE,(0)}} P_\ell \left(1 - \frac{r^2}{2d^2} \right) \sin kr. \tag{2·4}$$

Here, $C^{XX,\text{obs}}$ is the observed spectrum, and $b_\ell^{XX,(0)} \equiv C_\ell^{XX,\text{ex}(0)} / C_\ell^{XX,\text{app}(0)}$ is the ratio of the exact spectrum to an approximated spectrum calculated from a fiducial

spectrum $P^{(0)}(k)$, such as a scale-invariant one. This ratio b_ℓ^{XX} turns out to be almost independent of $P(k)$, and it therefore plays the role of a corrector of the errors caused by the approximations. The boundary conditions are given by the values of $P(k)$ at the zero points of $f(k)$ as

$$P(k_s) = \frac{S^{TT}(k_s) + \alpha S^{EE}(k_s)}{k_s \left[g^2(k_s) + \alpha h^2(k_s) \right]} \quad \text{for} \quad f(k_s) = 0, \tag{2.5}$$

assuming that $P'(k)$ is finite at $k = k_s$. In Eq. (2·2), the terms that have a prefactor of α come from the EE spectrum, and α controls the contribution of EE relative to TT. Because the positions of the singularities for TT and EE, given by $f(k) = 0$ and $h(k) = 0$, respectively, are different, if we choose an appropriate value of α such that the contribution of EE is comparable to that of TT, the solution of Eq. (2·2) becomes numerically stable, even in the neighborhoods of the singularities. We found such an appropriate value of α to be in the range $10^{13} - 10^{15}$ if there is no observational error.[16] As shown in a previous work, because of the tight coupling of the photon and baryon fluids at the LSS, the transfer function for EE, $h(k)$, is much smaller than those for TT, $f(k)$ and $g(k)$, by a factor of $\sim 10^{-7}$. The origin of the smallness of $h(k)$ is briefly explained in Appendix A. This is why the appropriate value of α is in the range $10^{13} - 10^{15}$.

Our original formalism described in Appendix A is based on a flat universe, where the spherical Bessel functions appear as the radial eigenfunctions of a Fourier expansion. Here, we extend our method to a nonflat universe. The dominant effect due to the curvature of the 3-geometry is effectively absorbed by adjusting the conformal distance to the LSS so that the angular diameter distance in a curved background is properly recovered. This gives rise to a shift of the Doppler peaks, with the overall shape of C_ℓ^{XX} unchanged. The shape of C_ℓ^{XX} changes mainly on large scales (at small ℓ), and its change on small scales is only a few percent.[19),20] Thus, under the small angle approximation, we need only modify d in $C_\ell^{XX,\,\mathrm{app}}$ depending on the curvature. This means that we can still use the spherical Bessel functions instead of the ultraspherical Bessel functions, which appear as the radial eigenfunctions in the curved background in $C_\ell^{XX,\,\mathrm{app}}$. In fact, we find that using the spherical Bessel functions causes only a small error that can be corrected by b_ℓ^{XX} and does not affect the resultant $P(k)$.

In conclusion, for a nonflat universe, we need no modification of our inversion formalism described in Appendix A, except for the adjustment of d, and the inversion formula (2·2) is applicable regardless of the geometry.

2.2. *Effect of observational errors*

Although in a previous paper[16] we showed that our method is effective if we assume that there is no observational error, it is also important to elucidate the effect of observational errors on the reconstructed $P(k)$. The existence of observational errors causes numerical errors to be amplified near the singularities, as shown in our recent work,[15] where we used only the TT spectrum. Therefore, we reconstructed $P(k)$ from C_ℓ^{XX} with observational errors, varying α, which represents the contribution of EE. We used the PLANCK observation and estimated the observational

errors, ΔC_ℓ^{XX}, by using the analytic formula[21]

$$\Delta C_\ell^{XX} = \sqrt{\frac{2}{(2\ell+1)f_{\mathrm{sky}}}} \left(C_\ell^{XX,\,\mathrm{real}} + 4\pi \frac{\sigma_{\mathrm{pix}}^2}{N_{\mathrm{pix}}} e^{\ell^2 \sigma_{\mathrm{beam}}^2} \right), \qquad (2\cdot 6)$$

where f_{sky} is the sky coverage ($f_{\mathrm{sky}}=1$ for a full-sky survey), N_{pix} is the number of pixels, σ_{pix} is the noise per pixel, σ_{beam} is the beam size, and $C_\ell^{XX,\,\mathrm{real}}$ is the real power spectrum. We set $f_{\mathrm{sky}} = 1$, $N_{\mathrm{pix}} = 2.3 \times 10^6$, $\sigma_{\mathrm{pix}} = 2.0\,\mu\mathrm{K}$ and $3.7\,\mu\mathrm{K}$ for TT and EE, respectively, and $\sigma_{\mathrm{beam}} = 0.13°$ for the PLANCK 143GHz channel.

First, for each ℓ, we drew a random number from a Gaussian distribution with ΔC_ℓ^{XX} around a theoretical C_ℓ^{XX}, and then reconstructed $P(k)$ from each simulated data set. Next, we estimated the mean and variance of the reconstructed $P(k)$ at each k for 1000 realizations. Our numerical calculations for evaluating C_ℓ^{XX} and the transfer functions are based on CMBFAST[*]. We used C_ℓ^{XX} up to $\ell_{\mathrm{max}} = 1500$ for both TT and EE. We assume a scale-invariant spectrum, $k^3 P(k) = \mathrm{const.}$, and set the cosmological parameters as $h = 0.70$, $\Omega_b = 0.050$, $\Omega_m = 0.30$, $\Omega_\Lambda = 0.70$, and $\tau = 0.20$. In this case, the positions of the TT singularities are at $kd \simeq 70, 430, 680, 1030, \cdots$, and those of the EE singularities are at $kd \simeq 230, 560, 860, 1180, \cdots$, where $d \simeq 1.36 \times 10^4\,\mathrm{Mpc}$. The range of the reconstructed $P(k)$ is between the first and fourth TT singularities, i.e., $70 \leq kd \leq 1030$, where kd roughly corresponds to ℓ. To focus on the effect of observational errors, we assume that the cosmological parameters are known precisely.

Figure 1 shows the results for $\alpha = 0$, 10^{14}, 5×10^{14}, and 10^{15}. We see that the error in $P(k)$ is very large near the TT singularities for $\alpha = 0$, which is also the case in the situation studied in our recent work.[15] However, as α is increased, near the TT singularities the error is reduced, while near the EE singularities it is amplified. For $\alpha = 5 \times 10^{14}$, the numerical error seems to be strongly suppressed near both the TT and EE singularities. On small scales (for $\ell \gtrsim 700$), the overall error in $P(k)$ becomes larger as α is increased, because the detector noise in C_ℓ^{EE} becomes the dominant source of error for the PLANCK observation. In the absence of observational errors, we showed that $P(k)$ is accurately reconstructed in the range $10^{13} \lesssim \alpha \lesssim 10^{15}$.[16] Taking the PLANCK observational errors into account, this range is narrowed due to the amplification of the numerical error, and the appropriate value of α is found to be $\sim 5 \times 10^{14}$, for which we can still suppress the numerical errors.

§3.   Constraining cosmological parameters

3.1.   *Method*

As mentioned in a previous paper,[16] it is in principle possible to constrain the cosmological parameters in our reconstruction method as follows. We need to examine the behavior of the reconstructed $P(k)$ when the free parameter α introduced in Eq. (2·2) is varied. We find that as long as we use the correct values of the cosmological parameters, $P(k)$ is accurately reconstructed for an appropriate value of α. On

---
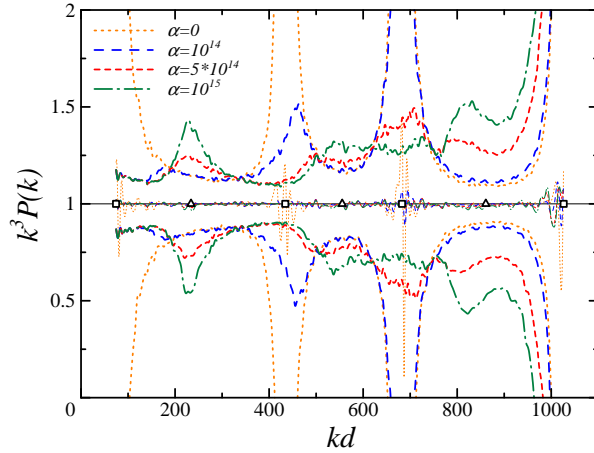
[*] http://www.cmbfast.org/

Fig. 1. Reconstructed spectra with observational errors. We assume a scale-invariant $P(k)$ and exactly known cosmological parameters, and we add the PLANCK observational errors to the theoretical C_ℓ^{TT} and C_ℓ^{EE}. The thin and thick curves represent the mean and variance, obtained from 1000 simulations, respectively. We plot them for four different values of α $(0, 10^{14}, 5 \times 10^{14},$ and $10^{15})$ which controls the contribution of EE relative to TT. The horizontal axis, kd, roughly corresponds to ℓ. The TT and EE singularities are represented by the symbols $\square$ and $\triangle$, respectively.

the other hand, if we use incorrect values, we obtain a particular deformed shape of the reconstructed $P(k)$ that depends on the value of α. To be more precise, if we use a relatively large value of α, the deformation appears near the EE singularities, while if we use a smaller value, the deformation appears near the TT singularities. The point is that such deformations caused by the incorrect choice of the cosmological parameters indicate not only deviations from the actual $P(k)$ but also inconsistent results for $P(k)$ among different values of α.

Let us denote the reconstructed $P(k)$ for a certain value of α by $P_\alpha(k)$ and introduce a quantity that represents the difference between $P_{\alpha_1}(k)$ and $P_{\alpha_2}(k)$. We define

$$D \equiv \int_{k_{\min}}^{k_{\max}} \frac{dk}{k} \left[k^3 P_{\alpha_1}(k) - k^3 P_{\alpha_2}(k) \right]^2, \qquad (3\cdot1)$$

where $\alpha_1 \neq \alpha_2$. From the above argument, we speculate that D takes its minimum value with respect to variation of the cosmological parameters at the correct values of these parameters. To confirm this speculation, we estimated the values of D for different values of the cosmological parameters, assuming that the values of these parameters used in §2.2 are the true values. We used C_ℓ^{XX} up to $\ell_{\max} = 1000$ for both TT and EE to avoid the effect of a large observational error. Hence, we take $k_{\min}$ and $k_{\max}$ to be the first and third TT singularities, respectively. We used $\alpha_1 = 10^{15}$ and $\alpha_2 = 10^{14}$, because these values are appropriate to suppress large numerical errors due to the singularities.

First, we assumed no observational error in C_ℓ^{XX} and estimated D as a function of the cosmological parameters. To see the dependence of $D = D(h, \Omega_b, \Omega_m, \Omega_\Lambda)$ on

$P(k)$, we performed calculations for three different shapes of $P(k)$. We adopted a scale-invariant $P(k)$, one with a large peak and dip, and one with a small oscillation. The spectrum with a peak and dip is expressed as

$$k^3 P(k) = A \left\{ 1 + a_1 \exp\left[-\frac{(k - k_1)^2}{\sigma_1^2} \right] \right\} \left\{ 1 + a_2 \exp\left[-\frac{(k - k_2)^2}{\sigma_2^2} \right] \right\}^{-1}, \quad (3\cdot2)$$

and we set $a_1 = a_2 = 1$, $k_1 = 0.03\,\mathrm{Mpc}^{-1}$, $k_2 = 0.06\,\mathrm{Mpc}^{-1}$, $\sigma_1 = 0.01\,\mathrm{Mpc}^{-1}$, and $\sigma_2 = 0.005\,\mathrm{Mpc}^{-1}$. The spectrum with an oscillation is expressed as

$$k^3 P(k) = A \left[1 + a_0 \sin\left(\frac{k}{k_0} \right) \right], \quad (3\cdot3)$$

and we set $a = 0.1$ and $k_0 = 5 \times 10^{-4}\,\mathrm{Mpc}^{-1}$. To elucidate the dependence of D on each cosmological parameter, we varied h, $\Omega_b h^2$, $\Omega_m h^2$, and $\Omega_K = 1 - \Omega_m - \Omega_\Lambda$ one at a time, keeping the others fixed to the assumed real values. Explicitly, we varied h from 0.60 to 0.80 with $\Delta h = 0.01$, keeping $\Omega_b h^2$, $\Omega_m h^2$, and Ω_K fixed; Ω_b from 0.040 to 0.060 with $\Delta \Omega_b = 0.001$, keeping h, $\Omega_m h^2$, and Ω_K fixed; Ω_m from 0.20 to 0.40 with $\Delta \Omega_m = 0.01$, keeping h, $\Omega_b h^2$, and Ω_K fixed; and Ω_Λ from 0.60 to 0.80 with $\Delta \Omega_\Lambda = 0.01$, keeping h, $\Omega_b h^2$, and $\Omega_m h^2$ fixed. Thus, the number of grid points is 21 in each case. Note that we fix the optical depth τ in our analysis, because it changes the shape of the spectrum only on large scales.

From the results shown in Fig. 2, we find that regardless of the shape of $P(k)$, D as a function of each cosmological parameter takes its minimum value at the correct value of that parameter in any case. With regard to the difference, the spectrum that has a large peak and dip tends to give larger values of D, while that with a small oscillation gives almost the same values as the scale-invariant spectrum. We also find that D is most sensitive to Ω_Λ or Ω_K. This is because the curvature affects the angular scale. It follows that the positions of the singularities, which correspond to the zero points of the transfer functions, shift to incorrect positions, and this causes large deviations of the reconstructed $P(k)$. As described in this section, we have confirmed that our method to constrain the cosmological parameters is effective as long as the observational error can be ignored. This method is quite intriguing, because it requires no assumption regarding the functional form of $P(k)$.

3.2. *Error estimation*

We also performed simulations to estimate the errors on the cosmological parameters in the case that we observe CMB anisotropies by the PLANCK satellite. We generated 1000 realizations with the PLANCK observational errors and reconstructed $P(k)$ from each realization in the same way as described in §2.2. For each realization, we calculated the value of D by varying the cosmological parameters and finding the minimum of D, which represents the location of the real values of the cosmological parameters, as discussed in the previous subsection. In practice, however, the location of the real values may be different from the minimum of D, due to observational errors. Therefore, we constructed histograms of the values of the cosmological parameters at the minimum of D from the 1000 realizations and estimated their probability distributions by Gaussian smoothing. The assumed model
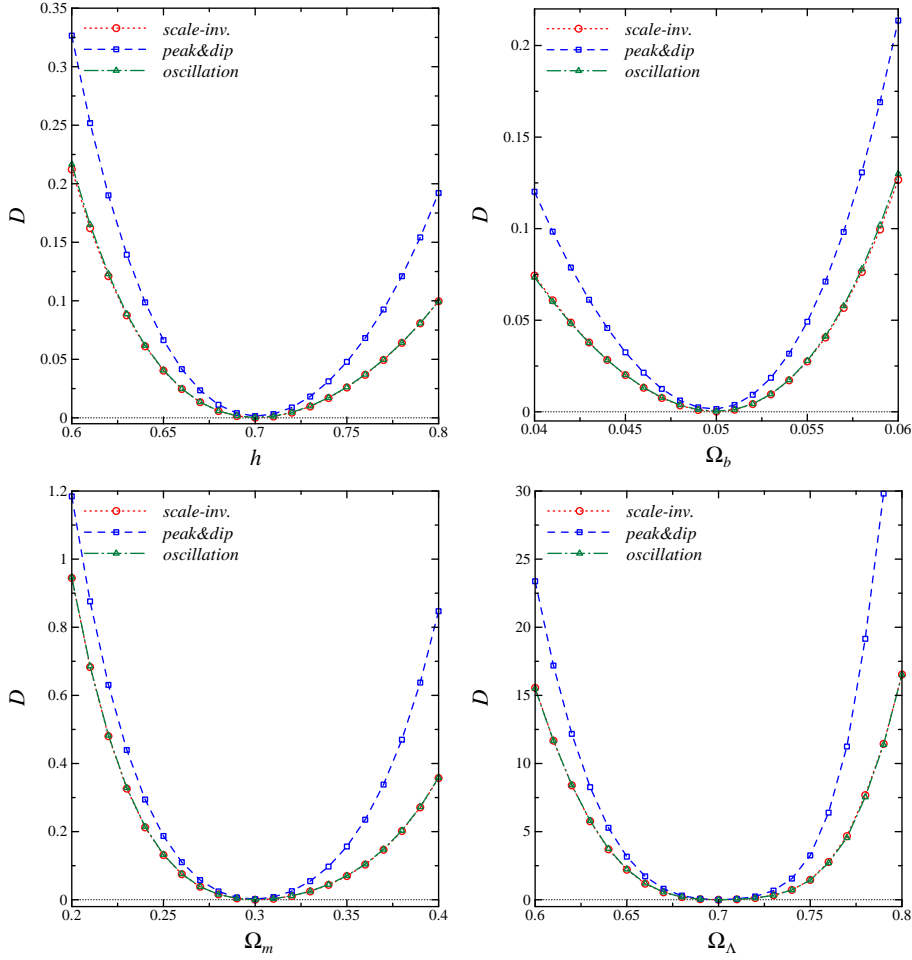
Fig. 2. D defined by Eq. (3·1) as a function of each cosmological parameter. In the separate plots
in each panel, we assume $P(k)$ as a scale-invariant spectrum, a spectrum with a peak and a dip,
and a spectrum with a small oscillation. The true cosmological parameters are assumed to be
$h = 0.70$, $\Omega_b = 0.050$, $\Omega_m = 0.30$, $\Omega_\Lambda = 0.70$, and $\tau = 0.20$. We vary h, $\Omega_b h^2$, $\Omega_m h^2$, and Ω_K,
keeping the others fixed at the assumed true values, in the top left, top right, bottom left, and
bottom right panels, respectively. (See the text for details.)

is a scale-invariant $P(k)$ with the same values of the cosmological parameters as used
in §2.2. Ultimately, we should perform a wide range parameter search in multiple
dimensions. However, here we used limited ranges for the possible values of the pa-
rameters and performed parameter searches only in one and two dimensions, mainly
because the purpose of this paper is to carry out preliminary examination of how
our basic strategy of unrestricting the functional form of $P(k)$ affects the parameter
estimation, and, practically, because our computations are quite time consuming.

First, we varied each cosmological parameter individually, keeping the others
fixed, as described in the previous subsection. The results are shown in Fig. 3. We
find that the probability distributions are nearly Gaussian, and their peaks lie near

the correct values in all cases, as expected, since we drew random numbers from Gaussian distributions around the theoretical C_ℓ^{XX} in our simulations, as mentioned in §2.2. For each cosmological parameter, we calculated its most probable value and the 1σ error from its estimated probability distribution. The result is given in Table I. We see that the most tightly constrained parameter is Ω_Λ or Ω_K, whose relative error is a few percent, provided that the other parameters are known and fixed. This is because D is most sensitive to the curvature, as mentioned in the previous subsection.

To see possible degeneracies among the cosmological parameters, we also performed two sets of two-dimensional analyses. In these analyses, we varied Ω_b and Ω_m, while keeping h and Ω_K fixed, and varied h and Ω_Λ, while keeping $\Omega_b h^2$ and $\Omega_m h^2$ fixed. To save computational time, we investigated the same range of the parameter space, but with bin sizes twice as large as the corresponding ones in the one-dimensional analyses. Thus, the number of grid points is 11×11. The results for Ω_b and Ω_m are shown in Fig. 4, and the estimated values of the cosmological parameters are listed in Table II. We find that in both cases the peaks deviate slightly from their correct values. In particular, the deviation from the correct value of Ω_b is quite large. As shown in Fig. 5, for h and Ω_Λ, there is a degeneracy caused by the fact that the same angular diameter distance can be the same for different sets of values of h and Ω_Λ.[22] We also see a peak near the correct values, but this peak is artificial, due to the sparseness of the parameter values we used. Moreover, the peaks in the projected probability distributions are amplified due to the narrowness of the parameter range, in which the global probability distribution does not converge sufficiently. For these reasons, we cannot estimate the values of the cosmological paramters from this analysis. We need more fine-meshed and wide-ranged parameter search, although the computational time becomes quite long in this case.

§4. Conclusion

In a previous work,[16] we proposed a method to reconstruct the primordial spectrum by using both the CMB temperature (TT) and the polarization (EE) spectra, and we showed that it is effective if there is no observational error. We also proposed a new method to constrain the cosmological parameters by using the fact that the shape of $P(k)$ obtained in this way must be independent of the contribution of EE relative to TT, which is controlled by the dimensionless parameter α. We found that the resulting $P(k)$ depends very strongly on α, unless the correct values of the cosmological parameters are used in the reconstruction. Using this fact, we can, in principle, constrain the cosmological parameters without any assumption on the functional form of $P(k)$.

In this paper, first, to elucidate the effect of observational error, we have reconstructed $P(k)$ from C_ℓ with the errors expected from PLANCK satellite observations, assuming that the cosmological parameters are known. As mentioned above, the contribution of EE relative to TT is parameterized by α. We have found that numerical errors due to the singularities corresponding to the zero points of the transfer functions are suppressed for $\alpha \sim 5 \times 10^{14}$, even when there exist observational errors. As
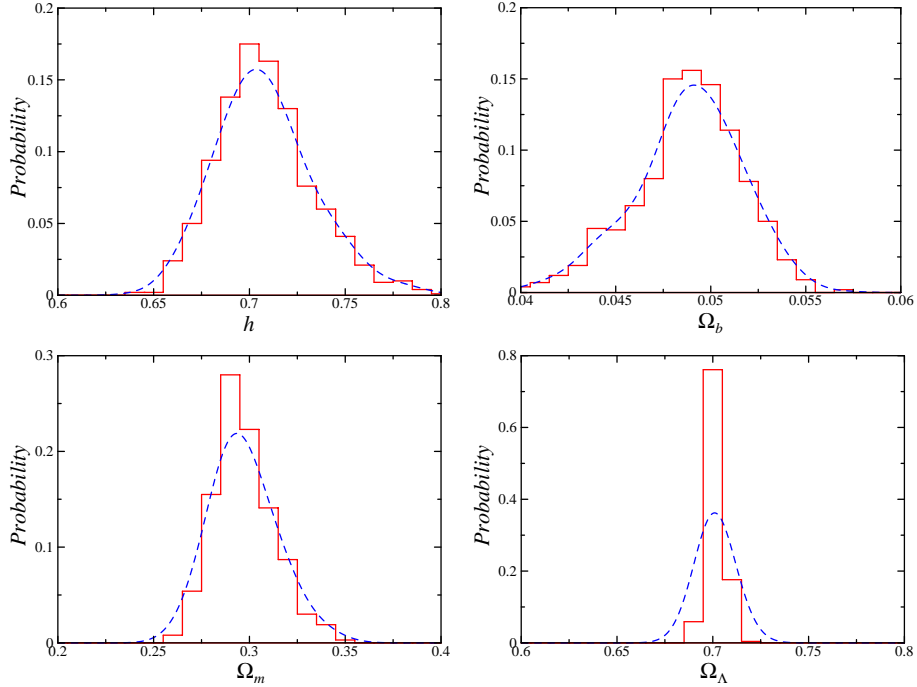
Fig. 3.   Probability distributions of the cosmological parameters estimated with the one-dimensional analyses. The histograms were obtained from 1000 simulations, and the dashed curves are the estimated probability distribution functions. The assumed model is a scale-invariant spectrum with the same cosmological parameters as in Fig. 2. The bin sizes for the parameters are $\Delta h = 0.01$, $\Delta \Omega_b = 0.001$, $\Delta \Omega_m = 0.01$, and $\Delta \Omega_\Lambda = 0.01$. We vary h, $\Omega_b h^2$, $\Omega_m h^2$, and Ω_K individually, keeping the others fixed, in the top left, top right, bottom left, and bottom right panels, respectively.

mentioned in a previous paper,[16] this value arises from the difference between the relative magnitudes of the transfer functions of TT and EE due to the tight coupling.

We have also investigated the possibility of constraining the cosmological parameters by using our inversion method, introducing the quantity D, which represents the difference between the reconstructed spectra for different values of α. In the ideal case with no observational error, we have shown that D takes its minimum value at the correct values of the cosmological parameters, independently of the shape of $P(k)$.

Then, to determine how tightly we can constrain the cosmological parameters in a realistic situation, we have performed simulations by taking the PLANCK observational errors into account. We generated 1000 realizations and determined the values of the cosmological parameters which minimize the value of D for each realization. By constructing histograms of these values, we estimated their probability distributions and 1σ errors. However, to save the computational time, we have performed only one- and two-dimensional analyses.

In the one-dimensional analysis, where we vary only one of the cosmological parameters at a time, with the others fixed at the assumed values, we found that
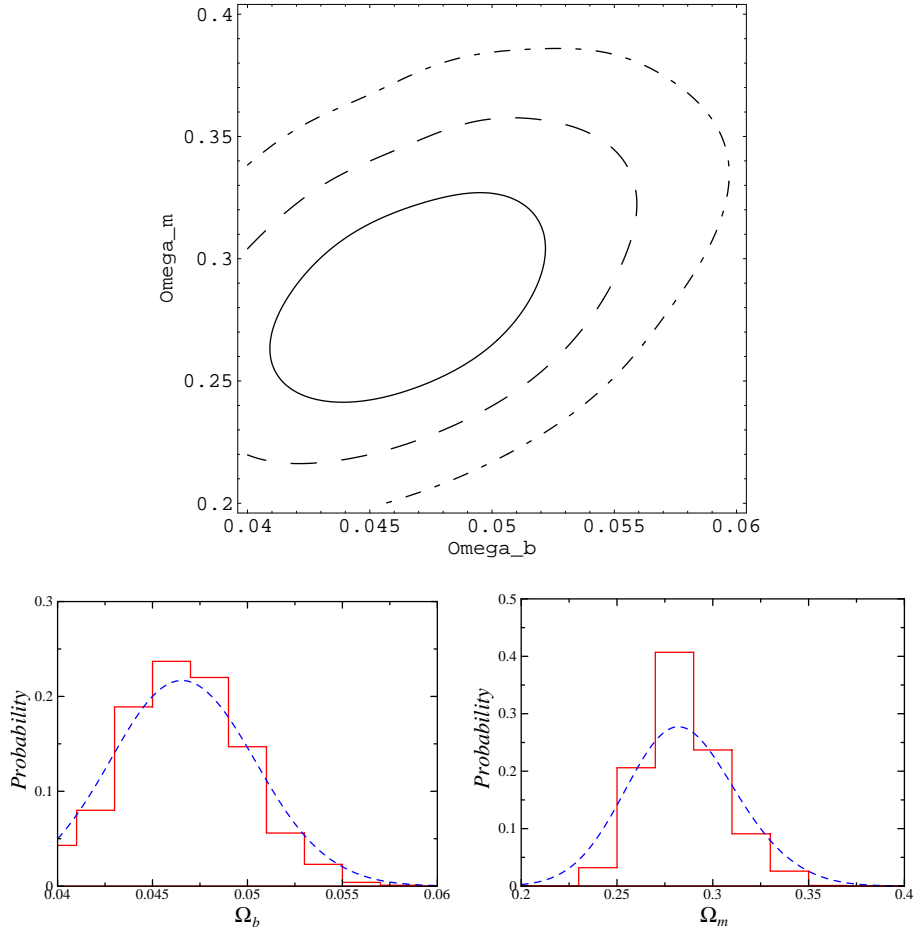
Fig. 4. Probability distributions of the cosmological parameters estimated with the two-dimensional analysis in (Ω_b, Ω_m) space. The assumed model is the scale-invariant spectrum with the same cosmological parameters as in Fig. 2. The bin sizes for the parameters are taken as $\Delta\Omega_b = 0.002$ and $\Delta\Omega_m = 0.02$. The values of h and Ω_K are fixed at the assumed values. The top panel shows the two-dimensional probability distribution, where the solid, dashed, and dash-dotted curves represent the 1σ, 2σ, and 3σ regions, respectively, and the bottom left and right panels show the projected probability distributions for Ω_b and Ω_m, respectively.

their probability distributions are nearly Gaussian, with the mean values close to the correct values. We also found that Ω_Λ is constrained most severely, with variances of a few percent relative to the mean values. This is because the variation of Ω_Λ is equivalent to the variation of Ω_K for fixed Ω_m, which significantly affects the angular diameter distance to the LSS, and an incorrect choice of Ω_Λ displaces the locations of the singularities in such a way that the consistency of the shapes of the TT and EE spectra is lost. This leads to a large value of D.

In the two-dimensional analysis, we have investigated two cases, one in which only Ω_b and Ω_m are varied, with h and Ω_K fixed, and one in which only h and Ω_Λ are varied, with $\Omega_b h^2$ and $\Omega_m h^2$ fixed. In the latter case, there is a degeneracy in
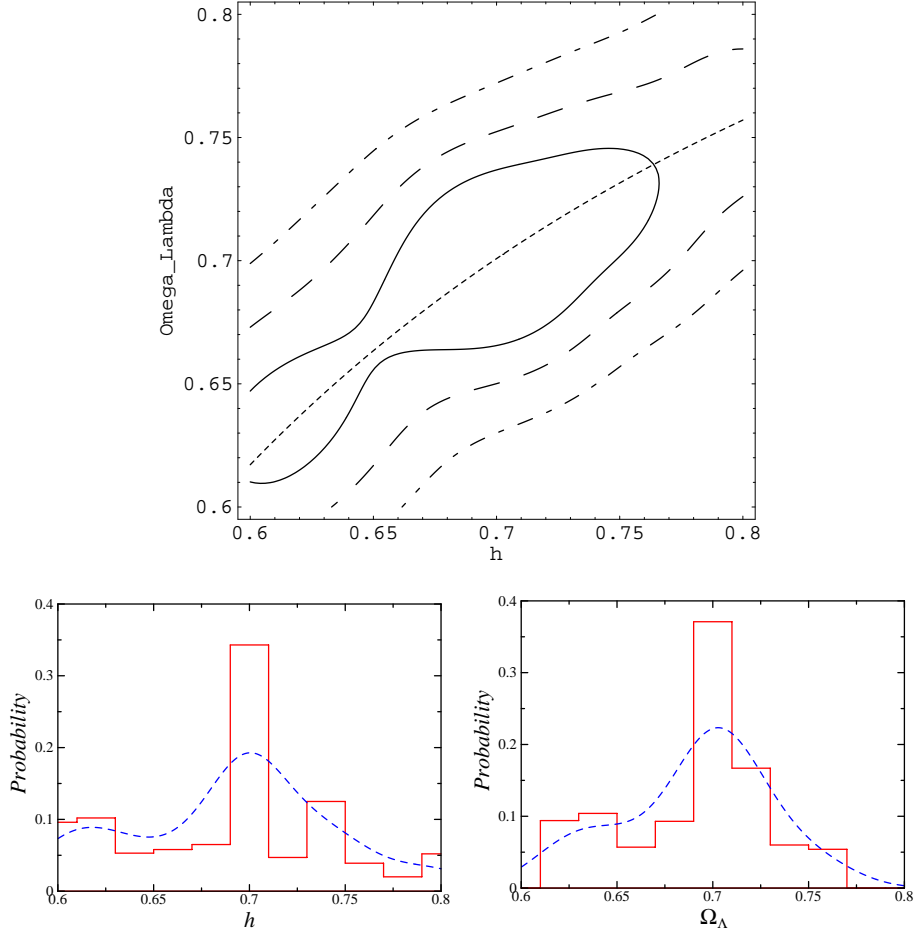
Fig. 5. Probability distributions of the cosmological parameters estimated with the two-dimensional analysis in (h, Ω_Λ) space. The assumed model is the scale-invariant spectrum with the same cosmological parameters as in Fig. 2. The bin sizes for the parameters are taken as $\Delta h = 0.02$ and $\Delta \Omega_\Lambda = 0.02$. We vary h and Ω_Λ, keeping $\Omega_b h^2$ and $\Omega_m h^2$ fixed. The top panel shows the two-dimensional probability distribution, where the solid, dashed, and dash-dotted curves represent the 1σ, 2σ, and 3σ regions, respectively, and the bottom left and right panels show the projected probability distributions for h and Ω_Λ, respectively. The short-dashed curve in the top panel represents the degeneracy curve, where the angular diameter distance is the same as that of the assumed model.

the (h, Ω_Λ) plane, because the angular diameter distance to the LSS, which determines the scale of the spectrum, depends on both h and Ω_Λ.[22] In our analysis, the sparse mesh and narrow parameter range caused an artificial peak in the probability distribution. Thus, we need to improve our computational method by optimizing the numerical code.

In any case, from the one-dimensional analysis, we may conclude that even if we allow an arbitrary functional form of $P(k)$, the cosmological parameters can be constrained by our inversion method, though this conclusion must be regarded as ten-

Table I. Estimated values of the cosmological parameters obtained from the probability distributions shown in Fig. 3.

	Assumed value	Estimated value	Fixed parameters
h	0.70	$0.703^{+0.027}_{-0.025}$	$\Omega_b h^2,\ \Omega_m h^2,\ \Omega_K,\ \tau$
Ω_b	0.050	$0.0491^{+0.0031}_{-0.0027}$	$h,\ \Omega_m h^2,\ \Omega_K,\ \tau$
Ω_m	0.30	$0.293^{+0.020}_{-0.017}$	$h,\ \Omega_b h^2,\ \Omega_K,\ \tau$
Ω_Λ	0.70	$0.701^{+0.011}_{-0.011}$	$h,\ \Omega_b h^2,\ \Omega_m h^2,\ \tau$

Table II. Estimated parameters obtained from the probability distributions shown in Fig. 4. Note that the range of Ω_b we investigated may not be large enough, as seen in Fig. 4.

	Assumed value	Estimated value	Fixed parameters
Ω_b	0.050	$0.0465^{+0.0037}_{-0.0036}$	$h,\ \Omega_K,\ \tau$
Ω_m	0.30	$0.282^{+0.030}_{-0.028}$	$h,\ \Omega_K,\ \tau$

tative, because we have explored only a limited range of the full, multi-dimensional parameter space in this paper.

It should be mentioned that the constraints obtained with our method are, of course, weaker than those obtained with the conventional parameter-fitting method if the primordial spectrum $P(k)$ exhibits a simple power-law form, as assumed in the latter. As the observational accuracy increases, however, there is a good chance that we will observe nontrivial effects of fundamental quantum physics[23]–[25] and/or non-slow-roll evolution of the inflation-driving scalar field.[26]–[29] These effects may impart complicated features on the primordial power spectrum that are beyond a simple power law. If this is indeed the case, we would not be able to obtain accurate values of the cosmological parameters using the conventional method, which restricts the spectral shape from the beginning. Our method would serve as a powerful tool in such a situation and could be more appropriate for the next generation of high-precision experiments, such as PLANCK, which are intended to provide data from which we can derive not only accurate values of the cosmological parameters but also a more precise shape of the primordial spectrum.

Acknowledgements

Appendix A
—— *Derivation of Inversion Formula* ——

Here we review our method of the reconstruction of $P(k)$ from both the CMB temperature and polarization spectra for scalar-type perturbations.[13),14),16)] We assume Gaussian and adiabatic primordial fluctuations. Although we restrict our discussions to a flat universe, it is easy to extend our formalism to a nonflat universe as mentioned in Sec. 2.1.

The angular power spectrum of the CMB anisotropy is expressed as

$$\frac{2\ell+1}{4\pi}C_\ell^{X\bar{X}} = \frac{1}{2\pi^2}\int_0^\infty \frac{dk}{k}\frac{k^3\langle X_\ell^*(\eta_0,k)\bar{X}_\ell(\eta_0,k)\rangle}{2\ell+1}, \tag{A·1}$$

where $X_\ell(\eta,k)$ and $\bar{X}_\ell(\eta,k)$ are either $\Theta_\ell(\eta,k)$ and $E_\ell(\eta,k)$ which represent multipole moments of temperature fluctuations and E-mode polarization in Fourier space, respectively. k is the comoving wavenumber and η is the conformal time with η_0 being the present value. These are expressed in the integral form of the Boltzmann equations ($\ell \geq 2$):[30)]

$$\frac{\Theta_\ell(\eta_0,k)}{2\ell+1} = \int_0^{\eta_0} d\eta \left\{ \left[(\Theta_0+\Psi)\mathcal{V}(\eta)+(\dot{\Psi}-\dot{\Phi})e^{-\tau(\eta)}\right]j_\ell(k\Delta\eta) \right.$$
$$\left. + V_b\mathcal{V}(\eta)j_\ell'(k\Delta\eta) + \frac{1}{2}\Pi_2\mathcal{V}(\eta)\left[3j_\ell''(k\Delta\eta)+j_\ell(k\Delta\eta)\right] \right\}, \tag{A·2}$$

$$\frac{E_\ell(\eta_0,k)}{2\ell+1} = -\frac{3}{2}\sqrt{\frac{(\ell+2)!}{(\ell-2)!}}\int_0^{\eta_0}d\eta\,\Pi_2\mathcal{V}(\eta)\frac{j_\ell(k\Delta\eta)}{(k\Delta\eta)^2}, \tag{A·3}$$

where $\Pi_2 \equiv (\Theta_2 - \sqrt{6}E_2)/10$, $\Delta\eta \equiv \eta_0 - \eta$, and the overdot denotes a derivative with respect to the conformal time. Here V_b is the baryon fluid velocity, Ψ and Φ are the Newton potential and the spatial curvature perturbation in the Newton gauge, respectively,[31)] and

$$\mathcal{V}(\eta) \equiv \dot{\tau}e^{-\tau(\eta)}, \quad \tau(\eta) \equiv \int_\eta^{\eta_0}\dot{\tau}d\eta, \tag{A·4}$$

are the visibility function and the optical depth for Thomson scattering, respectively. In the limit that the thickness of the last scattering surface (LSS) is negligible, we have $\mathcal{V}(\eta) \approx \delta(\eta-\eta_*)$ and $e^{-\tau(\eta)} \approx \theta(\eta-\eta_*)$, where η_* is the recombination time when the visibility function is maximum.[32)] To obtain a better approximation, we take into account the thickness of the LSS. This is required especially for the polarization, since the CMB polarization is mainly generated within the thickness of the LSS. The approximation is to neglect the oscillations of the spherical Bessel functions in the

integrals. Applying this approximation to Eqs. (A·2) and (A·3), we have

$$\frac{\Theta_\ell(\eta_0, k)}{2\ell+1} \approx \left\{ \int_{\eta_{*\text{start}}}^{\eta_{*\text{end}}} d\eta \left[(\Theta_0 + \Psi)\mathcal{V}(\eta) + (\dot{\Psi} - \dot{\Phi})e^{-\tau(\eta)} \right] \right\} j_\ell(kd)$$

$$+ \left\{ \int_{\eta_{*\text{start}}}^{\eta_{*\text{end}}} d\eta\, \Theta_1(\eta, k)\mathcal{V}(\eta) \right\} j'_\ell(kd) \equiv \frac{\Theta_\ell^{\text{app}}(\eta_0, k)}{2\ell+1}, \tag{A·5}$$

$$\frac{E_\ell(\eta_0, k)}{2\ell+1} \approx \sqrt{\frac{(\ell+2)!}{(\ell-2)!}} \left\{ -\frac{3}{2} \int_{\eta_{*\text{start}}}^{\eta_{*\text{end}}} d\eta\, \frac{\Pi_2}{(k\Delta\eta)^2}\mathcal{V}(\eta) \right\} j_\ell(kd) \equiv \frac{E_\ell^{\text{app}}(\eta_0, k)}{2\ell+1}, \tag{A·6}$$

where $d \equiv \eta_0 - \eta_*$ is the conformal distance from the present to the LSS and $\eta_{*\text{start}}$ and $\eta_{*\text{end}}$ are the times when the recombination starts and ends, respectively. We have also replaced V_b by Θ_1 and neglected the quadrupole term in Eq. (A·2), by adopting the tight coupling approximation.[32] We define time-integrated transfer functions within the thickness of the LSS, $f(k)$, $g(k)$, and $h(k)$ as

$$\int_{\eta_{*\text{start}}}^{\eta_{*\text{end}}} d\eta \left[(\Theta_0 + \Psi)(\eta, k)\mathcal{V}(\eta) + (\dot{\Psi} - \dot{\Phi})(\eta, k)e^{-\tau(\eta)} \right] \equiv f(k)\Phi(0, \boldsymbol{k}), \tag{A·7}$$

$$\int_{\eta_{*\text{start}}}^{\eta_{*\text{end}}} d\eta\, \Theta_1(\eta, k)\mathcal{V}(\eta) \equiv g(k)\Phi(0, \boldsymbol{k}), \tag{A·8}$$

$$-\frac{3}{2} \int_{\eta_{*\text{start}}}^{\eta_{*\text{end}}} d\eta\, \frac{\Pi_2(\eta, k)}{(k(\eta_0 - \eta))^2}\mathcal{V}(\eta) \equiv h(k)\Phi(0, \boldsymbol{k}). \tag{A·9}$$

Here we have separated terms of the transfer functions which are dependent only on the cosmological parameters, and the primordial curvature perturbation which leads the primordial power spectrum is defined as

$$P(k) \equiv \langle |\Phi(0, \boldsymbol{k})|^2 \rangle. \tag{A·10}$$

Let us compare the magnitudes of the transfer functions. At the recombination the quadrupole, dipole, and monopole are related as

$$\Theta_1 \sim \frac{k}{a_* H_*}(\Theta_0 + \Psi) \sim k\eta_*(\Theta_0 + \Psi) \sim kd\left(\frac{\eta_*}{\eta_0}\right)(\Theta_0 + \Psi), \tag{A·11}$$

$$\frac{\Pi_2}{(kd)^2} \sim \frac{1}{(kd)^2}\frac{k}{a_* n_e \sigma_T}\Theta_1 \sim \frac{k\eta_*}{(kd)^2}\frac{H_*}{n_e \sigma_T}\Theta_1 \sim \frac{1}{kd}\left(\frac{\eta_*}{\eta_0}\right)\left(\frac{H_*}{n_e \sigma_T}\right)\Theta_1, \tag{A·12}$$

where n_e is the number density of free electrons, σ_T is the cross section of the Thomson scattering, and the subscript $*$ denotes the value at the recombination. Since $\eta_*/\eta_0 \sim 0.02$ and the mean free time of the Thomson scattering is much shorter than the cosmic expansion time, $H_*/(n_e\sigma_T) \sim 10^{-3}$,[31] $\Theta_1 \sim 10^{-2}(kd)(\Theta_0 + \Psi)$ and $\Pi_2/(kd)^2 \sim 10^{-5}(kd)^{-1}\Theta_1$. Thus, at $kd \sim \ell \sim O(10^2)$, $f(k) \sim g(k) \sim 10^7 h(k)$.

Substituting Eqs. (A·5) and (A·6) into Eq. (A·1), we obtain the approximated TT, EE, and TE angular power spectra,

$$\frac{2\ell+1}{4\pi}C_\ell^{TT, \text{app}} = \frac{2\ell+1}{2\pi^2} \int_0^\infty \frac{dk}{k} k^3 P(k) \left[f(k)j_\ell(kd) + g(k)j'_\ell(kd) \right]^2, \tag{A·13}$$

$$\frac{2\ell+1}{4\pi}C_\ell^{EE,\text{app}} = \frac{2\ell+1}{2\pi^2}\frac{(\ell+2)!}{(\ell-2)!}\int_0^\infty \frac{dk}{k}\,k^3 P(k)\,[h(k)j_\ell(kd)]^2\,, \tag{A·14}$$

$$\frac{2\ell+1}{4\pi}C_\ell^{TE,\text{app}} = \frac{2\ell+1}{2\pi^2}\sqrt{\frac{(\ell+2)!}{(\ell-2)!}}$$

$$\times\int_0^\infty \frac{dk}{k}\,k^3 P(k)\left[f(k)j_\ell(kd)+g(k)j_\ell'(kd)\right]h(k)j_\ell(kd). \tag{A·15}$$

The angular correlation function of the CMB temperature fluctuations is defined as

$$C^{TT}(\theta)\equiv\langle\Theta(\hat{\boldsymbol{n}}_1)\Theta(\hat{\boldsymbol{n}}_2)\rangle = \sum_{\ell=0}^\infty \frac{2\ell+1}{4\pi}C_\ell^{TT}P_\ell(\cos\theta),\quad \cos\theta=\hat{\boldsymbol{n}}_1\cdot\hat{\boldsymbol{n}}_2\,. \tag{A·16}$$

Similarly, we introduce the following quantities for the polarization:

$$\tilde{C}^{EE}(\theta)\equiv\sum_{\ell=0}^\infty \frac{2\ell+1}{4\pi}\frac{(\ell-2)!}{(\ell+2)!}\,C_\ell^{EE}P_\ell(\cos\theta), \tag{A·17}$$

$$\tilde{C}^{TE}(\theta)\equiv\sum_{\ell=0}^\infty \frac{2\ell+1}{4\pi}\sqrt{\frac{(\ell-2)!}{(\ell+2)!}}\,C_\ell^{TE}P_\ell(\cos\theta), \tag{A·18}$$

which are not the conventional angular correlation functions but they turn out to be convenient for inversion. Here we introduce a new variable r instead of θ defined as

$$r = 2d\sin\frac{\theta}{2}, \tag{A·19}$$

which is the conformal distance between two points on the LSS. From now on, we focus only on small angular scales, corresponding to $r \ll d$, which is valid where $\ell \gtrsim O(10)$. For the TT spectrum, substituting Eq. (A·13) into Eq. (A·16), we can derive formulas for the approximated angular correlation functions in terms of $P(k)$. With the help of the Fourier sine formula, we obtain a first-order differential equation for $P(k)$,

$$-k^2 f^2(k)P'(k) + \left[-2k^2 f(k)f'(k)+kg^2(k)\right]P(k)$$

$$= 4\pi\int_0^\infty dr\,\frac{1}{r}\frac{\partial}{\partial r}\{r^3 C^{TT,\text{app}}(r)\}\sin kr \equiv S^{TT}(k). \tag{A·20}$$

This is the basic equation for the inversion of the TT angular power spectrum to the primordial curvature perturbation spectrum. Although the above differential equation is singular at $f(k)=0$ since the transfer functions are oscillatory, we can find the values of $P(k)$ at such points, say $k=k_s$, as

$$P(k_s) = \frac{S^{TT}(k_s)}{k_s\,g^2(k_s)}\quad\text{for}\quad f(k_s)=0, \tag{A·21}$$

assuming that $P'(k)$ is finite at $k=k_s$. We can then solve Eq. (A·20) as a boundary value problem between the singularities. Similarly, for the EE and TE spectrum,

substituting Eqs. (A·14) and (A·15) into Eqs. (A·17) and (A·18), respectively, and so on, we obtain the algebraic equations for $P(k)$,

$$kh^2(k)P(k) = 4\pi \int_0^\infty dr\, r \tilde{C}^{EE,\,\mathrm{app}}(r) \sin kr \equiv S^{EE}(k), \tag{A·22}$$

$$kf(k)h(k)P(k) = 4\pi \int_0^\infty dr\, r \tilde{C}^{TE,\,\mathrm{app}}(r) \sin kr \equiv S^{TE}(k). \tag{A·23}$$

In this case, we can find $P(k)$ except for the singularities of $h(k) = 0$ for EE, and those of $f(k) = 0$ and $h(k) = 0$ for TE, respectively. These are the basic inversion formulas for the EE and TE angular power spectra. If we use inversion formulas (A·20), (A·22) and (A·23) separately, the reconstructed $P(k)$ suffers from large numerical errors around the singularities of the respective equations. However, the fact that the zero points of $f(k)$ and $h(k)$ are different from each other can be used to resolve this numerical problem as follows. We construct a combined inversion formula by multiplying Eq. (A·22) by some factor α and adding it to Eq. (A·20),

$$-k^2 f^2(k)P'(k) + \left[-2k^2 f(k)f'(k) + kg^2(k) + \alpha kh^2(k) \right] P(k)$$
$$= S^{TT}(k) + \alpha S^{EE}(k). \tag{A·24}$$

The boundary conditions are similarly given by the values of $P(k)$ at zero points of $f(k)$ as

$$P(k_s) = \frac{S^{TT}(k_s) + \alpha S^{EE}(k_s)}{k_s \left[g^2(k_s) + \alpha h^2(k_s) \right]} \quad \text{for} \quad f(k_s) = 0, \tag{A·25}$$

assuming that $P'(k)$ is finite at $k = k_s$. Here we have taken α to be independent of k for simplicity and this free parameter α controls the contribution of EE relative to TT. If we take an appropriate value of α so that the contribution of EE is comparable to that of TT, the solution of Eq. (A·24) becomes numerically stable even around the singularities. This is because the contribution of EE dominates near the singularities of TT given by $f(k) = 0$, and vice versa. We have found such an appropriate value of α is $\sim 10^{13} - 10^{15}$ if we assume no observational error.[16] The origin of this number comes from the fact that the transfer function $h(k)$ for EE is intrinsically smaller than the transfer functions $f(k)$ and $g(k)$ for TT by a factor $\sim 10^{-7}$ as explained above and their squares are contained in the left-hand side of Eq. (A·24). Since the TE formula, Eq. (A·23), which is singular not only at $h(k) = 0$ but also at $f(k) = 0$, is difficult to handle, we do not use it so far.

For either TT or EE, the approximated spectrum $C_\ell^{XX,\,\mathrm{app}}$ ($X = T$ or E) expressed as Eq. (A·13) or (A·14) has relative errors as large as about $20 - 30\%$ to the exact one $C_\ell^{XX,\,\mathrm{ex}}$ expressed as Eq. (A·1). Unless we correct such errors due to the approximation, it leads wrong $P(k)$ when solving Eq. (A·24) which uses the observed spectrum $C_\ell^{XX,\,\mathrm{obs}}$. Therefore, we introduce the ratio,

$$b_\ell^{XX} \equiv \frac{C_\ell^{XX,\,\mathrm{ex}}}{C_\ell^{XX,\,\mathrm{app}}}. \tag{A·26}$$

This ratio is found to be almost independent of $P(k)$. We explain the reason as follows. In both $C_\ell^{XX,\,\mathrm{ex}}$ and $C_\ell^{XX,\,\mathrm{app}}$, the transfer functions including the spherical Bessel functions are rapidly oscillating functions compared to a reasonable $P(k)$ for sufficiently large ℓ. Thus, when we take the ratio, the dependence on $P(k)$ effectively cancels out. We use this property of b_ℓ^{XX} with some fiducial primordial spectrum $P^{(0)}(k)$ such as a scale-invariant one. That is, we first calculate $b_\ell^{XX,\,(0)} = C_\ell^{XX,\,\mathrm{ex}(0)}/C_\ell^{XX,\,\mathrm{app}(0)}$, from $P^{(0)}(k)$, and then we use $C_\ell^{XX,\,\mathrm{obs}}/b_\ell^{XX,\,(0)}$ which gives a better guess to $C_\ell^{XX,\,\mathrm{app}}$, instead of $C_\ell^{XX,\,\mathrm{obs}}$, in the right-hand side of Eq. (A·24). As a result, we obtain $P(k)$ with much better accuracy.

Finally, substituting Eqs. (A·16) and (A·17) into Eq. (A·24) and replacing $C_\ell^{XX,\,\mathrm{app}}$ by $C_\ell^{XX,\,\mathrm{obs}}/b_\ell^{XX,\,(0)}$, we obtain the inversion formula (2·2) in Sec. 2.1.

References

1) C. L. Bennett *et al.*, Astrophys. J. Lett. **464** (1996), L1.
2) C. L. Bennett *et al.*, Astrophys. J. Suppl. **148** (2003), 1.
3) E. Komatsu *et al.*, Astrophys. J. Suppl. **148** (2003), 119.
4) D. N. Spergel *et al.*, Astrophys. J. Suppl. **148** (2003), 175.
5) H. Peiris *et al.*, Astrophys. J. Suppl. **148** (2003), 213.
6) P. Mukherjee and Y. Wang, Astrophys. J. **598** (2003), 779.
7) P. Mukherjee and Y. Wang, Astrophys. J. **599** (2003), 1.
8) P. Mukherjee and Y. Wang, astro-ph/0502136.
9) S. L. Bridle, A. M. Lewis, J. Weller and G. Efstathiou, Mon. Not. R. Astron. Soc. **342** (2003), L72.
10) S. Hannestad, J. Cosmol. Astropart. Phys. **04** (2004), 002.
11) A. Shafieloo and T. Souradeep, Phys. Rev. D **70** (2004), 043523.
12) D. Tocchini-Valentini, M. Douspis and J. Silk, astro-ph/0402583.
13) M. Matsumiya, M. Sasaki and J. Yokoyama, Phys. Rev. D **65** (2002), 083007.
14) M. Matsumiya, M. Sasaki and J. Yokoyama, J. Cosmol. Astropart. Phys. **02** (2003), 003.
15) N. Kogo, M. Matsumiya, M. Sasaki and J. Yokoyama, Astrophys. J. **607** (2004), 32.
16) N. Kogo, M. Sasaki and J. Yokoyama, Phys. Rev. D **70** (2004), 103001.
17) T. Souradeep, J. R. Bond, L. Knox, G. Efstathiou and M. S. Turner, astro-ph/9802262.
18) W. H. Kinney, Phys. Rev. D **63** (2001), 043001.
19) W. Hu and M. White, Astrophys. J. **471** (1996), 30.
20) M. Zaldarriaga, U. Seljak and E. Bertschinger, Astrophys. J. **494** (1998), 491.
21) L. Knox, Phys. Rev. D **52** (1995), 4307.
22) G. Efstathiou and J. R. Bond, Mon. Not. R. Astron. Soc. **304** (1999), 75.
23) J. Martin and R. H. Brandenberger, Phys. Rev. D **63** (2001), 123501.
24) R. H. Brandenberger and J. Martin, Mod. Phys. Lett. A **16** (2001), 999.
25) J. Martin and R. Brandenberger, Phys. Rev. D **68** (2003), 063513.
26) A. A. Starobinsky, JETP Lett. **55** (1992), 489.
27) J. Yokoyama, Phys. Rev. D **59** (1999), 107303.
28) S. M. Leach and A. R. Liddle, Phys. Rev. D **63** (2001), 043508.
29) J. A. Adams, B. Cresswell and R. Easther, Phys. Rev. D **64** (2001), 123514.
30) U. Seljak and M. Zaldarriaga, Astrophys. J. **469** (1996), 437.
31) H. Kodama and M. Sasaki, Prog. Theor. Phys. Suppl. **No.78** (1984), 1.
32) W. Hu and N. Sugiyama, Astrophys. J. **444** (1995), 489.